Additional changes and corrections

A1. Additional simulation over the continental United States (CONUS)

We recently finished a whole month simulation covering CONUS including the newly developed glyoxal SOA module within the framework of a model intercomparison. This simulation provides insight into the greater significance of SOA from glyoxal in other regions and strengthens the suspicion we articulated in the last sentence in the manuscript's conclusions ("We expect that especially the Eastern US is very susceptible to glyoxal SOA formation due to high relative humidity, high availability of all precursors as well as substantial aerosol concentrations.", p 29, l 14-16). We hence included this simulation result in the manuscript. The manuscript has been rewritten on several occasions to accommodate the additional simulations. We only reproduce those changes here that extend the scientific result of the manuscript.

A paragraph has been added before the conclusions:

4.5 SOA from glyoxal over the continental US

We employed the model system as described above, using the VOLUME parameterization for glyoxal-SOA formation, to conduct a simulation over the continental US for the whole month of July 2010. Thereby we could investigate the contribution of glyoxal to SOA at the continental scale. In Figure 15 we show the average concentration of gas-phase glyoxal and SOA from glyoxal in the lowest model level. While glyoxal-SOA concentrations over the western and central US are low, the eastern part of the US exhibits concentrations of up to 0.8 ug m-3 (15% of total SOA) with the highest values located over Ohio/Pennsylvania. Gas-phase glyoxal concentrations over the northeastern US are comparable to the ones over California, yet the northeastern US has higher concentrations of glyoxal-SOA. As we showed above, the gas-particle transfer of glyoxal (and hence SOA production from glyoxal) is hampered under dry conditions by a kinetic limitation in the increase in Henry's law constant.
The comparison between the Northeast and California clearly shows this effect: while precursor concentrations are comparable, the amount of SOA produced from glyoxal is higher in the Northeast, as pollution levels there provide ample aerosol volume (and inorganic salts) to shift substantial amounts of glyoxal to the particle-phase while the humid conditions keep the salt concentrations in deliquesced particles below the levels where the kinetic limitation would come into play.

The conclusions have been rewritten (see revised manuscript) and now contain a paragraph about the results of the CONUS simulation

p 26701 l 27ff:
Results from the month-long 36 km resolution simulation over the domain of the Continental United States revealed that the Eastern, and especially the Northeastern US, is more susceptible to SOA formation from glyoxal through volume pathways. This is despite comparable levels of gas-phase glyoxal are observed in California. We explain this by the fact that the formation of SOA from glyoxal is kinetically limited in the Western US due to dry conditions and high salt concentrations in the aerosol which hamper the gas-particle transfer of glyoxal.

A figure has been added (Figure 15):

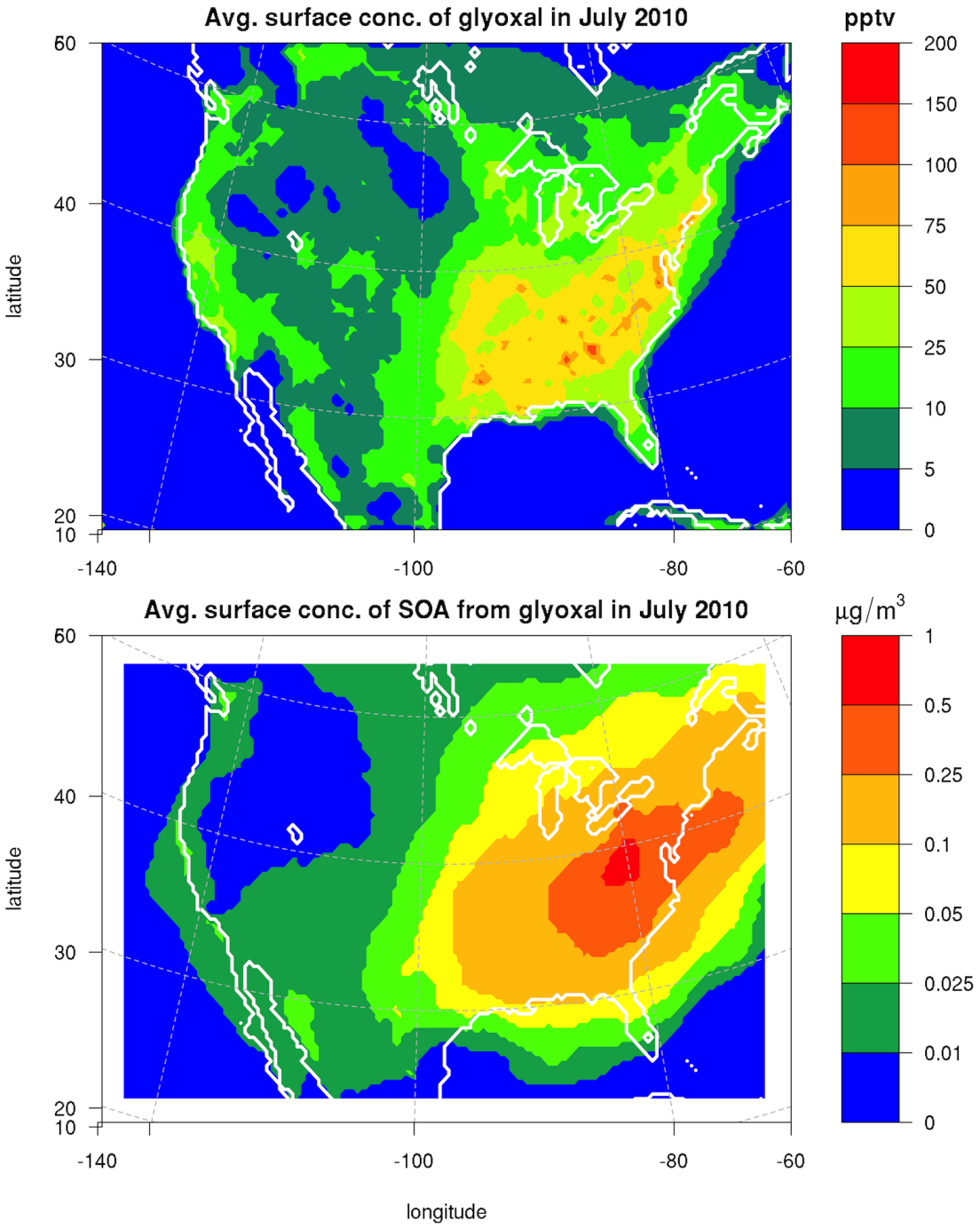

Figure 15. Average surface level concentration of gas-phase glyoxal (top) and SOA from glyoxal (bottom) in July 2010 over the continental United States. Simulation based on the VOLUME parameterization.

A2. MBO chemistry

Explicit MBO (2-methyl-3-buten-2-ol) chemistry was not included in the MOZART mechanism, MBO emissions (and subsequent chemistry) were lumped with isoprene. There is evidence that MBO is a major precursor to glyoxal in the Eastern Slopes of the Central Valley (e.g. Huisman et al., 2011), and that omitting this glyoxal production pathway could have important effects on our results due to the different glyoxal yields. We hence included MBO oxidation chemistry and repeated all simulations. However, the resulting differences were minor as we find that the oxidation pathways lead to very similar glyoxal concentrations and the MBO emissions by MEGAN are substantially lower than the one of isoprene. We nonetheless included this new chemistry into the description as it will be part of the updated MOZART mechanism and can hence be referenced by others.

Paragraph 2.3.1 has been updated:

p 26708, l 2-4:
Four main formation pathways are considered: oxidation of isoprene, of aromatic compounds, of MBO (2-methl-3-buten-2-ol) and of ethyne.

p 26708, l 18-19:

not significant sources of glyoxal. MBO chemistry, initiated via reaction with OH, NO3 and ozone, is also added to the model. Note that glycolaldehyde is a significant product of the OH-initiated oxidation of MBO, and that further reactions of glycolaldehyde lead to glyoxal production. Ethyne has also been added

The last sentence of paragraph 2.3.1 has been removed.

Tables 3, 4 and 5 have been amended:

Table 3. Continued.

Symbolic name	Atomic composition	Comments
MBO	$CH_2{=}CH{-}C(OH)(CH_3)_2$	2-methyl-3-buten-2-ol
MBOO2	$HOCH_2{-}CH(OO){-}C(OH)(CH_3)_2$	Peroxy radical from OH + MBO
MBONO3O2	$O_2NOCH_2{-}CH(OO){-}C(OH)(CH_3)_2$	Peroxy radical from NO_3 + MBO
MBOOOH	$HOCH_2{-}CH(OOH){-}C(OH)(CH_3)_2$	Dihydroxy-hydroperoxide formed in reaction of MBOO2 with HO_2
HMPROP	$(CH_3)_2C(OH)CH{=}O$	2-hydroxy-2-methyl-propanal
HMPROPO2	$(CH_3)_2C(OH)C(O)OO$	Peroxy radical formed from OH + HMPROP reaction

Table 4. Continued.

Reactants		Products	Rate Constant(s)
MBO + OH	→	MBOO2	8.1E−12 · exp(610/T)
MBO + O3	→	.1 CO + .5 CH2O + .1 CH3COCH3 + .9 HMPROP + .25 HCOOH + .25 CO + .06 HO2 + .06 OH	1.0E−17
MBO + NO3	→	MBONO3O2	4.6E−14 · exp(−400/T)
MBOO2 + NO	→	HO2 + .67 GLYALD + .67 CH3COCH3 + .33 HMPROP + .33 CH2O + NO2	2.6E−12 · exp(365/T)
MBOO2 + CH3O2	→	.917 CH2O + HO2 + .25 CH3OH + .333 GLYALD + .333 CH3COCH3 + .167 HMPROP	3.75E−13 · exp(−40/T)
MBOO2 + HO2	→	MBOOOH	7.5E−13 · exp(−700/T)
MBONO3O2 + HO2	→		4.3E−13 · exp(1040/T)
MBONO3O2 + NO	→	.25 HMPROP + .25 CH2O + 1.25 NO2 + .75 ONIT + .75 CH3COCH3 + .75 HO2	2.6E−12 · exp(365/T)
MBONO3O2 + NO3	→	.25 HMPROP + .25 CH2O + 1.25 NO2 + .75 ONIT + .75 CH3COCH3 + .75 HO2	2.4E−12
MBOOOH + OH	→	.5 MBOO2 + .5 OH	3.8E−12 · exp(200/T)
HMPROP + OH	→	HMPROPO2	1.4E−11
HMPROPO2 + NO	→	NO2 + HO2 + CH3COCH3 + {CO2}	2.6E−12 · exp(365/T)
HMPROPO2 + HO2	→	.4 OH + .4 HO2 + .4 CH3COCH3 + {.4 · CO2}	4.3E−13 · exp(1040/T)

Table 5. New photolysis reactions. (J_X is the photolysis rate for compound X calculated by fTUV.)

Reactant		Products	Rate
$HONO + h\nu$	$\rightarrow$	$OH + NO$	J_{HONO}
$BIGALD1 + h\nu$	$\rightarrow$	$.6 \cdot MALO2 + HO2$	$0.140 \cdot J_{NO_2}$
$BEPOMUC + h\nu$	$\rightarrow$	$BIGALD1 + 1.5 \cdot HO2 + 1.5 \cdot CO$	$0.100 \cdot J_{NO_2}$
$TEPOMUC + h\nu$	$\rightarrow$	$.5 \cdot CH3CO3 + HO2 + 1.5 \cdot CO$	$0.100 \cdot J_{NO_2}$
$BIGALD2 + h\nu$	$\rightarrow$	$.6 \cdot HO2 + .6 \cdot DICARBO2$	$0.200 \cdot J_{NO_2}$
$BIGALD3 + h\nu$	$\rightarrow$	$.6 \cdot HO2 + .6 \cdot CO + .6 \cdot MDIALO2$	$0.200 \cdot J_{NO_2}$
$BIGALD4 + h\nu$	$\rightarrow$	$HO2 + CO + CH3COCHO + CH3CO3$	$0.006 \cdot J_{NO_2}$
$MBOOOH + h\nu$	$\rightarrow$	$OH + HO2 + .67 \cdot GLYALD + .67 \cdot CH3COCH3$ $+ .33 \cdot HMPROP + .33 \cdot CH2O$	$J_{CH_3O_2H}$
$HMPROP + h\nu$	$\rightarrow$	$2 \cdot HO2 + CO + CH3COCH3$	J_{GLYALD}

A4. Minor text changes

We added citations to datasets and the supercomputing facility used to conduct the simulations (p 7, l 20ff):

All simulations are initialized and forced at the lateral boundaries by 6 hourly analysis data from the NCEP Global Forecast System (GFS) at 1.0◦ resolution for meteorology (NCEP, 2000), and 6 hourly MOZART-GEOS5 simulations (based on Emmons et al., 2010) at 1.9×2.5◦ resolution for chemistry and aerosols. Simulations are nudged to GFS analyses above the boundary layer throughout the simulation. Sea surface temperature (SST) analyses updated every 6 hours from the US Navy Fleet Numerical Meteorology and Oceanography Center (http: //www.usgodae.org/ftp/outgoing/fnmoc/models/ghrsst/docs/ghrsst doc.txt) are used instead of default climatologies. The simulations were conducted using the NCAR high performance computing system "Yellowstone" (CISL , 2000).

p 26717 l 4-5: reflect that measurements indicate that the photolysis sink is larger than reaction with OH
The main sinks for glyoxal in the model are reaction with OH, photolysis, and dry and wet deposition.

removed "a" from "a detailed"
p 26701 l 7 **WRF-Chem to include detailed gas-phase chemistry**

moved references to end of sentence p 26702 l 15-18.
Laboratory measurements for glyoxal confirmed that it partitions into the particle phase under atmospheric conditions due to its high solubility in water and its subsequent aqueous-phase chemistry (Kroll et al., 2005; Liggio et al., 2005; Carlton et al., 2007; Noziere et al., 2009; Galloway et al., 2009; Volkamer et al., 2009).

added reference p 26704 l 6-8:
[...] and emissions of compounds related to SOA formation like VOCs (Borbon et al., 2013), NOx (McDonald et al., 2012; Brioude et al., 2013; Baidar et al., 2013b), or ammonia (Nowak et al., 2012).

Figure 7 caption: **Comparison against vertical profiles of glyoxal as measured by AMAX-DOAS (black) on 15 June (low approach over Bakersfield (Baidar et al., 2013b) at about 21:25–21:40 UTC.**

We made clear that Kampf et al. (2013) measured “salting-in” based on ammonium sulfate particles and effects of other salts are currently unknown. We further clarified that we assume ammonium nitrate behaves like ammonium sulfate with respect to its effect on the Henry’s law constant of glyoxal, and that this is not part of Kampf et al., 2013:

p 26709 l 15ff **[...] where K_h, water = 4.19 × 10^5 M atm^{-1} is the Henry’s law constant of glyoxal over water, −0.24 the “salting-in” constant of ammonium sulfate, and cas and can the concentrations (mol kg^{-1}) of ammonium sulfate and nitrate respectively. Kampf et al. (2013) derived the “salting-in” constant for ammonium sulfate, constants for other seed particles are currently unmeasured. In this work we assume that ammonium nitrate acts like ammonium sulfate and their effects are additive. The sum c_{as} + c_{an} in the calculation above is limited to 12 mol kg^{-1} , per the results of Kampf et al. (2013), who found no further increase in $K_{h,eq}$ at higher concentrations (of ammonium sulfate) within the time scales of their experiments. [...]**

p 26709 l 24 - p 26710, l 5: Kampf et al. (2013) determined that K_{olig} is approximately unity, for c_{as} <12 mol kg^{-1} and 0.5 for c_{as} >12 mol kg^{-1}. They also showed a significant time-dependence of the rate at which the Henry’s law equilibrium is established. In particular, the characteristic time scales for gas-particle partitioning of monomer species (glyoxal,monohydrate,and dihydrate) is on the order of minutes at c_{as} <12 mol kg^{-1}, and several hours at c_{as} >12 mol kg^{-1}.

p 26710 l 11-12: Using the values derived in (Kampf et al., 2013) for ammonium sulfate particles, we assume again that ammonium nitrate behaves like ammonium sulfate and use $\langle tau \rangle_1$ =2.5×10^2s for (c_{as} +c_{an}) < 12M, and 4.4×10^4s for (c_{as}+c_{an})>12M.

p 26710 l 19-20. **In this work $\langle tau \rangle_2$ = 5.5×10^3 s for (c_{as} +c_{an}) < 12 mol kg^{-1}, and 4.7×10^4 s for (c_{as}+c_{an}) > 12 mol kg^{-1} (based on values for ammonium sulfate in Kampf et al., 2013).**

p 26720 l 8 - 11: **(ii) The increase in the Henry's law constant for the reversible processes depends exponentially on the total concentration of ammonium sulfate in deliquesced aerosols, with an upper limit at 12 mol kg^{-1} (Kampf et al., 2013). A substantial area of the model domain is above this limit on average, especially if we assume (as done in this work) that ammonium nitrate has the same effect as ammonium sulfate and that their effects are additive.This indicates that 'potential'**

for SOA formation from glyoxal is suppressed kinetically, possibly as a result of the increasing particulate viscosity at very high salt concentrations.

conclusions: **[...] HYBRID uses both, as do FAST and FAST_PH. The latter two simulations are pure sensitivity studies, as there is no laboratory evidence so far to remove the kinetic limitation, and no basis to increase the pH value. Measurements of the effect of salts other than ammonium sulfate on the Henry's law constant of glyoxal are currently not available and would be desirable to further our understanding of glyoxal-SOA formation. Given that VOLUME is based on explicitly identified pathways [...]**

Added reference to pH calculations based on measurements and explicit thermodynamic modeling, p 26719 l 14: **The pH of aerosol particles ranges between 1.5 and 5 and is typically around 3.5, close to the values of 3.88 +/- 0.34 (mean and std) derived by explicit thermodynamic modeling of the conditions at the LA ground site presented in Liu et al. (2012a).**

Corrected factor used to describe range glyoxal-SOA spans:
p 26701 l 28ff: **[...] and we conclude that the current uncertainty on glyoxal SOA formation spans a factor of 15 in the LA basin for this time period.**

p 26722 l 15: **Comparison of the different formation pathways reveals that glyoxal SOA formed through the volume pathways alone (VOLUME) is a factor of 15 lower than from an irreversible reactive surface uptake (SIMPLE) [...]**

p 26724 l 23: **Depending on the pathways considered, glyoxal contributes between 1 and 15 % to total SOA mass in the LA basin [...]**

p 26723 l 2-3: the sentence "**Simulation chamber data [...]**" has been removed.

reformulated paragraph p 26723 l 10 - 16 to make it more readable: **The FAST_PH simulation was a sensitivity study to investigate the partitioning behaviour in regions where the aerosol pH is higher on average. In Mexico City the higher pH strongly increases the contribution of glyoxal to SOA (Waxman et al., 2013). However, we find only minor increases over FAST over California, where the limiting factor is not the ammonium-catalyzed reaction rate (Eq. 5), but the availability of glyoxal in the particle phase. This illustrates the strong impact that a kinetic limitation in reversible partitioning has on inhibiting the rate of glyoxal-SOA formation over California.**

Additional references used

Huisman, A. J., Hottle, J. R., Galloway, M. M., DiGangi, J. P., Coens, K. L., Choi, W., Faloona, I. C., Gilman, J. B., Kuster, W. C., de Gouw, J., Bouvier-Brown, N. C., Goldstein, A. H., LaFranchi, B. W., Cohen, R. C., Wolfe, G. M., Thornton, J. A., Docherty, K. S., Farmer, D. K., Cubison, M. J., Jimenez, J. L., Mao, J., Brune, W. H., and Keutsch, F. N.: Photochemical modeling of glyoxal at a rural site: observations and analysis from BEARPEX 2007, Atmos. Chem. Phys., 11, 8883-8897, doi:10.5194/acp-11-8883-2011, 2011.